

Long lifetime hole traps at grain boundaries in CdTe thin-film photovoltaics

BG Mendis^{1*}, D Gachet², JD Major³ and K Durose³

1. *Dept. of Physics, Durham University, South Road, Durham, DH1 3LE, UK*
2. *Attolight AG, EPFL Innovation Square, Building D, 1015 Lausanne, Switzerland*
3. *Stephenson Institute for Renewable Energy, University of Liverpool, Chadwick Building, Liverpool, L69 7ZF, UK*

* Corresponding author (b.g.mendis@durham.ac.uk)

Abstract

A novel time-resolved cathodoluminescence method, where a pulsed electron beam is generated via the photoelectric effect, is used to probe individual CdTe grain boundaries. Excitons have a short lifetime (≤ 100 ps) within the grains and are rapidly quenched at the grain boundary. However, a ~ 47 meV shallow acceptor, believed to be due to oxygen, can act as a long lifetime hole trap, even at the grain boundaries where their concentration is higher. This provides direct evidence supporting recent observations of hopping conduction across grain boundaries in highly doped CdTe at low temperature.

Text

The record cell efficiency for CdTe thin-film photovoltaics is currently 21.0% [1] despite the presence of grain boundaries. To achieve a high efficiency a chlorine activation step is required, during which chlorine segregates along CdTe grain boundaries [2-3], thereby potentially passivating any deep recombination energy levels. A higher room temperature carrier lifetime following chlorine activation was measured throughout the material, including predominantly grain boundary regions, using time-resolved photoluminescence (TRPL) in a confocal microscope [4]. Electron beam induced current (EBIC) imaging in a scanning electron microscope (SEM) has shown bright contrast at grain boundaries indicating that they are preferential sites for current collection [3,5]. However, the method is subject to complex effects, such as high electron injection densities which can lead to bright grain boundary contrast [6]. Spatially resolved photoluminescence at liquid nitrogen temperature has also uncovered a long range (>10 μm) hopping transport mechanism across grain boundaries [7]. Hopping conduction takes place via impurity trap levels that give rise to the ~ 1.4 eV donor acceptor pair (DAP) peak in the CdTe luminescence spectrum. Since the samples had a high Cu content (10^{19} cm^{-3}) due to a $\text{Cu}_{1.4}\text{Te}$ adhesive layer the impurity was assumed to be a Cu_{Cd} acceptor ~ 146 meV above the valence band maximum (VBM) [8]. A relatively long lifetime of ~ 25 ns was measured for the DAP peak, consistent with long range hole transport [7].

Experiments on carrier recombination at grain boundaries are complicated by the simultaneous requirement of high spatial and temporal resolution. TRPL has good temporal resolution and although two-photon excitation can be used to improve the spatial resolution [9] it is generally inferior to SEM. Bimberg and co-workers [10] on the other hand have used

beam blanking in an SEM to carry out time-resolved cathodoluminescence (TRCL) studies on GaAs. Although the carrier lifetime across individual dislocations was successfully measured [11] the temporal resolution (≤ 200 ps) is inadequate for probing the fast recombination channels anticipated in thin-film photovoltaic materials. An alternative method is to generate an electron pulse via laser excitation of a photocathode, as first demonstrated by Merano *et al* [12]. The spatial and temporal resolution are estimated at 10 nm and 10 ps respectively, and is therefore ideal for investigating individual grain boundaries. Carrier lifetime is a critical parameter for high efficiency photovoltaic devices (e.g. [13]) and its measurement at high spatial resolution, particularly at defects such as grain boundaries, has application beyond CdTe to other thin-film materials such as Cu(In,Ga)Se₂ and Cu₂ZnSn(S,Se)₄. Here we report the first results on grain boundaries in CdTe, an exemplar thin-film photovoltaic.

Devices were fabricated by close space sublimation of 99.999% pure CdTe onto radio frequency sputtered CdS at 575 °C for 60 mins. These conditions were chosen to produce large CdTe grains for cathodoluminescence analysis. The high deposition temperature causes some thinning of the CdS layer, thereby reducing device efficiency [14]. The cell was activated by evaporating a 200 nm thick layer of CdCl₂ on the CdTe back surface and annealing in air at 440 °C for 20 mins, to give an efficiency of 5.1% [14]. Further details can be found in the supplementary information [25]. A small area (2 x 1 mm²) of the CdTe back surface was polished to a smooth surface finish for SEM using 1 keV energy Ar-ions at 2° incidence angle. Measurements were carried out on an Attolight ‘Chronos’ quantitative cathodoluminescence (CL) microscope operating at 6 keV beam energy. The field emission gun could be used either as a conventional electron source (i.e. continuous wave, CW) or as a photocathode to generate electron pulses. For the latter a frequency doubled Ti:sapphire laser with 80 MHz repetition rate was used to excite the photocathode. The TRCL signal was detected on a Hamamatsu C5680 streak camera with a time gate of 2.1 ns. Time integrated CL spectra were detected on a Horiba Synapse CCD camera in either CW or pulsed modes. The sample was cryogenically cooled, using liquid-He, to 12 K (see supplementary information [25]).

First the results from hyperspectral mapping in continuous wave CL (CW CL) mode are presented. Figure 1a shows the panchromatic intensity of the chlorine activated CdTe sample. CL spectra from the grain labelled ‘G1’ and the neighbouring grain boundary (‘GB’) are shown in Fig. 1b. The total intensities have been normalised for direct comparison. The near band edge region consists of an acceptor bound exciton (A^oX) at 779 nm (1.592 eV). A further peak is observed at 797 nm (1.556 eV); recent studies [15-16] have shown this to be two closely spaced peaks of an electron to acceptor (eA^o ; 795 nm or 1.559 eV) and donor acceptor pair (DAP; 799 nm or 1.552 eV) transitions involving a common acceptor. Evidence for these assignments is based on the temperature evolution of the two peaks. With increasing temperature the DAP peak decays first, due to ionisation of the shallow donor level, while the eA^o transition remains till ~ 30 K [15-16]. From the low temperature band gap for CdTe (1.606 eV [17]) the acceptor level is estimated to be ~ 47 meV above the VBM [16]. The acceptor has been associated with oxygen [15, 18-19], based on the observation that the peak intensity increases with oxygen concentration. Note that *neutral* Cd-vacancies have also been proposed as an acceptor [20], but is thought to be unlikely since the intrinsic charge is -2.

Oxygen can be introduced during several stages of device fabrication, such as impurities in the starting material, vacuum break between CdS and CdTe deposition, residual gases in the close space sublimation chamber and especially during chloride activation which is normally done in air. The same peak was also observed in the sample prior to activation [21]. A second DAP peak is observed over a broad wavelength range (~850-950 nm) and has been associated with copper and also with chlorine impurities, such as the chlorine A-centre [22]. In this letter the two DAP peaks are labelled as DAP₁ and DAP₂ for convenience (Fig. 1f).

Figures 1c, 1d and 1e show the intensity distribution of the A^oX, eA^o/DAP₁ and DAP₂ transitions, after normalising with respect to the total CL signal, so that grain boundary regions, with high non-radiative recombination, can be directly compared with grain interiors. Bound excitons are quenched at grain boundaries, while the opposite is true for the two other transitions. However, some grains interiors (e.g. G3 in Fig. 1d) show a high intensity for the eA^o/DAP₁ transition, which suggests that the shallow acceptor has a non-uniform spatial distribution. A Gaussian curve was fitted to the DAP₂ transition and its central wavelength plotted as a function of position in Fig. 1f. The DAP₂ peak is blue shifted at the grain boundaries compared to the grain interiors; this is also evident in Fig. 1b where the peak shift between GB and G1 is ~14 nm. A higher normalised intensity and blue shift is consistent with a smaller donor acceptor pair spacing and indicates that the grain boundaries are sinks for the impurities involved.

Results from pulsed excitation CL are presented in Figure 2. Fig. 2a shows the time integrated CL spectra extracted from the grain interior 'G1' and grain boundary 'GB' (Fig. 1a). Compared to CW CL the A^oX exciton peak in pulsed mode is suppressed with respect to the other transitions, especially at the grain boundary. Some insight into its origin is obtained from the DAP₂ peak position, which in pulsed mode is similar for both the grain interior and grain boundary, and has a similar value to the grain boundary in CW mode. The temporal width of the electron pulses is less than 10 ps, so that the instantaneous power is much larger than in CW CL, causing ionised donors and acceptors to readily capture free carriers (the first step in eA^o and DAP recombination), a process that appears to be more efficient than exciton formation. This results in a relative increase in eA^o, DAP intensities, as well as blue shifting of the DAP₂ peak within the grain interior to the 'saturation' value corresponding to small donor-acceptor pair spacings. The DAP₂ blue shift between the two modes is 26 meV for the grain interior 'G1'. A ~6 meV/decade blue shift has been reported for the ~1.3 eV DAP 'Z-band' in CdTe [16], so that the power density could be increasing by several orders of magnitude in pulsed mode (see supplementary information [25]). The eA^o/DAP₁ peak position is however similar for both continuous and pulsed CL modes, although the results of [19] suggests a blue shift of ~1 meV/decade. The peak could therefore be dominated by the eA^o transition and/or the DAP pair separation could be relatively large. The normalised intensity distributions for the A^oX, eA^o/DAP₁ and DAP₂ transitions showed some of the features in Fig. 1, although the results were less conclusive, presumably due to the high injection conditions (see supplementary information [25]).

The time resolved decay curves for the A^oX peak at the grain interior 'G1' and grain boundary 'GB' are shown in Fig. 2b. The former has two lifetimes, as revealed by plotting the intensity on a logarithmic scale. The decay curve was least squares fitted to a function of

the form $[A_1 \exp(-t/\tau_1) + A_2 \exp(-t/\tau_2)]$, where A_1 , A_2 are constants and τ_1 , τ_2 are the lifetimes. The ‘dark’ intensity at time $t < 0$ was subtracted prior to fitting, since there was a strong correlation between this and other variables, leading to erroneous results. The values obtained for τ_1 and τ_2 are 44 ps and 100 ps respectively (error < 0.1 ps), while $A_1/A_2 = 269$, indicating that the former is dominant. The neighbouring grain interior ‘G2’ (Fig. 1a) yielded similar results (i.e. $\tau_1 = 37$ ps, $\tau_2 = 74$ ps and $A_1/A_2 = 999$). The lifetime τ_1 is assumed to be that of a free exciton; the small value as well as the fact that the free exciton peak is not visible in the CL spectrum suggests that recombination is primarily non-radiative. On the other hand the longer lifetime τ_2 is assumed to be that of the A^0X exciton, which is formed when a free exciton binds to a neutral acceptor, so that it can avoid non-radiative recombination centres, and therefore decay radiatively after a longer time delay. The higher density of non-radiative recombination centres at a grain boundary means that the ‘GB’ curve in Fig. 2b is dominated by τ_1 ($= 31 \pm 9$ ps), with the longer lifetime decay virtually absent. Monte Carlo simulations were carried out to determine the effect of surface recombination on the measured lifetimes. For large surface recombination velocities ($\geq 10^5$ cm/s) the longer lifetime τ_2 will be underestimated, while τ_1 is less affected (see supplementary information [25]). The short exciton lifetime is consistent with photoluminescence measurements [7].

The eA^0/DAP_1 decay rate is considerably slower both at the grain interior ‘G1’ and grain boundary ‘GB’ (Fig. 2c). The intensity prior to excitation is larger than the dark spectrum with the beam turned off, indicating that emission lasts longer than the 12.5 ns laser repetition period. This is also true of other sample regions (see supplementary information [25]). Interestingly, emission starts to increase after ~ 1 ns following pulse excitation (see arrows in Fig. 2c). Examination of CL spectra at different time intervals show that the initial decay is due to a loss of intensity from the short wavelength region (i.e. to the left of the eA^0/DAP_1 intensity maximum), while the increase after 1 ns is due to stronger emission at longer wavelengths (i.e. to the right of the maximum); see supplementary information [25]. This could probably be due to the eA^0 and DAP_1 transitions of small pair spacings taking place rapidly, while DAP_1 transitions of larger pair spacings, which have lower recombination probability, take place after a time delay. In fact different transition rates for eA^0 and DAP_1 recombination has been observed in GaAs, with the result that the transient spectrum evolves with time [10]. Nevertheless the interpretation must be treated with caution, since the long decay time could distort the measured streak camera signal. Furthermore, the lack of sensitivity of the streak camera at long wavelengths meant that it was not possible to measure decay curves for the DAP_2 transition.

As mentioned earlier long range carrier transport across grain boundaries has been observed in CdTe, due to hopping conduction via the ~ 146 meV Cu_{Cd} acceptor states [7]. Although the sample in that study had a high Cu content (10^{19} cm $^{-3}$) hopping conduction has also been reported for CdTe with 10^{17} cm $^{-3}$ carrier concentration [23]. It is not clear if our sample exhibits hopping transport (there was no intentional Cu doping) but the results demonstrate that the ~ 47 meV shallow acceptor level is an efficient hole trap and can therefore assist in hopping transport at large dopant concentrations. Hole trapping is also detected at grain boundaries, where the acceptor has a higher concentration (Fig. 1d), despite the fact that the lower CL intensity at the grain boundary indicates higher levels of non-radiative

recombination (Fig. 1a; [24]). Hole traps at the grain boundary provide a conduction pathway for hopping transport across neighbouring grains, as first observed by Alberi *et al* [7].

It should be clarified that hopping conduction is a low temperature phenomenon, as confirmed by mobility measurements [7, 23]. In fact the eA^0/DAP_1 transition is absent at temperatures above ~ 30 K due to thermal ionisation of the shallow acceptor [15-16]. Room temperature continuous wave CL spectra of a CdTe grain interior and grain boundary are shown in Figure 3a. The intense peak at 818 nm (1.516 eV; arrowed) is close to the room temperature band gap [17]. There is a significant amount of *above* band gap emission, the relative fraction of which is higher at the grain boundaries (Fig. 3c). The above band gap intensity is due to free electron-hole recombination, while exciton recombination and phonon emission constitute the near-band edge and below band gap intensity [17]. The decrease of the 818 nm peak intensity at the grain boundaries (Fig. 3b) suggests that excitons are quenched at the grain boundaries, similar to low temperature (Fig. 2b). Luminescence due to trap states is not detected, consistent with full thermal ionisation of impurities at 300 K. Non-radiative recombination via deep defect states, which is not revealed by CL, is therefore likely to be the critical factor for photovoltaic performance under normal operating conditions.

In summary the carrier dynamics of individual CdTe grain boundaries at liquid-He temperature has been successfully probed using a novel time-resolved cathodoluminescence technique. Excitons are rapidly quenched at the grain boundaries. A shallow acceptor, ~ 47 meV above the valence band maximum, is present throughout the material and at higher concentration at the grain boundaries. The acceptor is thought to be due to oxygen impurities and is a long lifetime hole trap, even at the grain boundaries. This provides valuable insight into the long range hopping conduction mechanism previously reported in highly doped CdTe at low temperature.

Acknowledgements

EPSRC funding for BGM (EP/K001620/1) and KD (EP/J017361/1) is gratefully acknowledged. The following DOI can be used to access the data- doi:10.15128/j3860693n.

References

- [1] M.A. Green, K. Emery, Y. Hishikawa, W. Warta and E.D. Dunlop, *Prog. Photovolt: Res. Appl.* **23**, 1 (2015).
- [2] M. Terheggen, H. Heinrich, G. Kostorz, A. Romeo, D. Baetzner, A.N. Tiwari, A. Bosio and N. Romeo, *Thin Solid Films* **431-432**, 262 (2003).
- [3] J.D. Poplawsky, N.R. Paudel, C. Li, C.M. Parish, D. Leonard, Y. Yan and S.J. Pennycook, *Adv. Energy Mater.* **V**, 1400454 (2014).
- [4] C. Kraft, H. Hempel, V. Buschmann, T. Siebert, C. Heisler, W. Wesch and C. Ronning, *J. Appl. Phys.* **113**, 124510 (2013).
- [5] C. Li, Y. Wu, J. Poplawsky, T.J. Pennycook, N. Paudel, W. Yin, S.J. Haigh, M.P. Oxley, A.R. Lupini, M. Al-Jassim, S.J. Pennycook and Y. Yan, *Phys. Rev. Lett.* **112**, 156103 (2014).

- [6] S.A. Galloway, P.R. Edwards and K. Durose, *Solar Energy Mat. Solar Cells* **57**, 61 (1999).
- [7] K. Alberi, B. Fluegel, H. Moutinho, R.G. Dhere, J.V. Li and A. Mascarenhas, *Nature Comm.* **4**, 2699 (2013).
- [8] W. Stadler, D.M. Hofman, H.C. Alt, T. Muschik, B.K. Meyer, E. Weigel, G. Müller-Vogt, M. Salk, E. Rupp and K.W. Benz, *Phys. Rev. B* **51**, 10619 (1995).
- [9] J. Ma, D. Kuciauskas, D. Albin, R. Bhattacharya, M. Reese, T. Barnes, J.V. Li, T. Gessert and S-H. Wei, *Phys. Rev. Lett.* **111**, 067402 (2013).
- [10] D. Bimberg, H. Münzel, A. Steckenborn and J. Christen, *Phys. Rev. B* **31**, 7788 (1985).
- [11] A. Steckenborn, H. Münzel and D. Bimberg, *J. of Luminescence* **24-25**, 351 (1981).
- [12] M. Merano, S. Sonderegger, A. Crottini, S. Collin, P. Renucci, E. Pelucchi, A. Malko, M. H. Baier, E. Kapon, B. Deveaud and J.-D. Ganière, *Nature* **438**, 479 (2005).
- [13] T.A. Gessert, S.H. Wei, J. Ma, D.S. Albin, R.G. Dhere, J.N. Duenow, D. Kuciauskas, A. Kanevce, T.M. Barnes, J.M. Burst, W.L. Rance, M.O. Reese and HR Moutinho, *Solar Energy Mat. Solar Cells* **119**, 149 (2013).
- [14] A.A. Taylor, J.D. Major, G. Kartopu, D. Lamb, J. Duenow, R.G. Dhere, X. Maeder, S.J.C. Irvine, K. Durose and B.G. Mendis, *Solar Energy Mat. Solar Cells* **141**, 341 (2015).
- [15] J Van Gheluwe, J Versluys, D Poelman and P Clauws, *Thin Solid Films* **480-481**, 264 (2005).
- [16] C Kraft, H Metzner, M Häudrich, U Reislöhner, P Schley, G Gobsch and R Goldhahn, *J. Appl. Phys.* **108**, 124503 (2010).
- [17] J Lee, NC Giles, D Rajavel and CJ Summers, *Phys. Rev. B* **49**, 1668 (1994).
- [18] MA Hernández-Fenollosa, DP Halliday, K Durose, MD Campo and J Beier, *Thin Solid Films* **431-432**, 176 (2003).
- [19] K Akimoto, H Okuyama, M Ikeda and Y Mori, *Appl. Phys. Lett.* **60**, 91 (1992).
- [20] D Grecu, AD Compaan, D Young, U Jayamaha and DH Rose, *J. Appl. Phys.* **88**, 2490 (2000).
- [21] AA Taylor, JD Major, K Durose and BG Mendis, unpublished results.
- [22] DM Hoffmann, P Omling, HG Grimmeiss, BK Meyer, KW Benz and D Sinerius, *Phys. Rev. B* **45**, 6247 (1992).
- [23] RP Sharma, AK Shukla, AK Kapoor, R Srivastava and PC Mathur, *J. Appl. Phys.* **57**, 2026 (1985).
- [24] BG Mendis, L Bowen and QZ Jiang, *Appl. Phys. Lett.* **97**, 092112 (2010).
- [25] See Supplemental Material [url], which includes Refs. [14, 26-30].
- [26] JD Major, YY Proskuryakov, K Durose, G Zoppi and I Forbes, *Solar Energy Mat. Solar Cells* **94**, 1107 (2010).
- [27] DC Joy, *Monte Carlo Modelling For Electron Microscopy and Microanalysis*, Oxford University Press (1995).
- [28] CA Klein, *J. Appl. Phys.* **39**, 2029 (1968).
- [29] M Gloeckler, AL Fahrenbruch and JR Sites (2003) Proc. 3rd World Conference PVSEC, Osaka, Japan, pp 491-494.
- [30] T Schmidt, K Lischka and W Zulehner, *Phys. Rev. B* **45**, 8989 (1992).

Figure captions

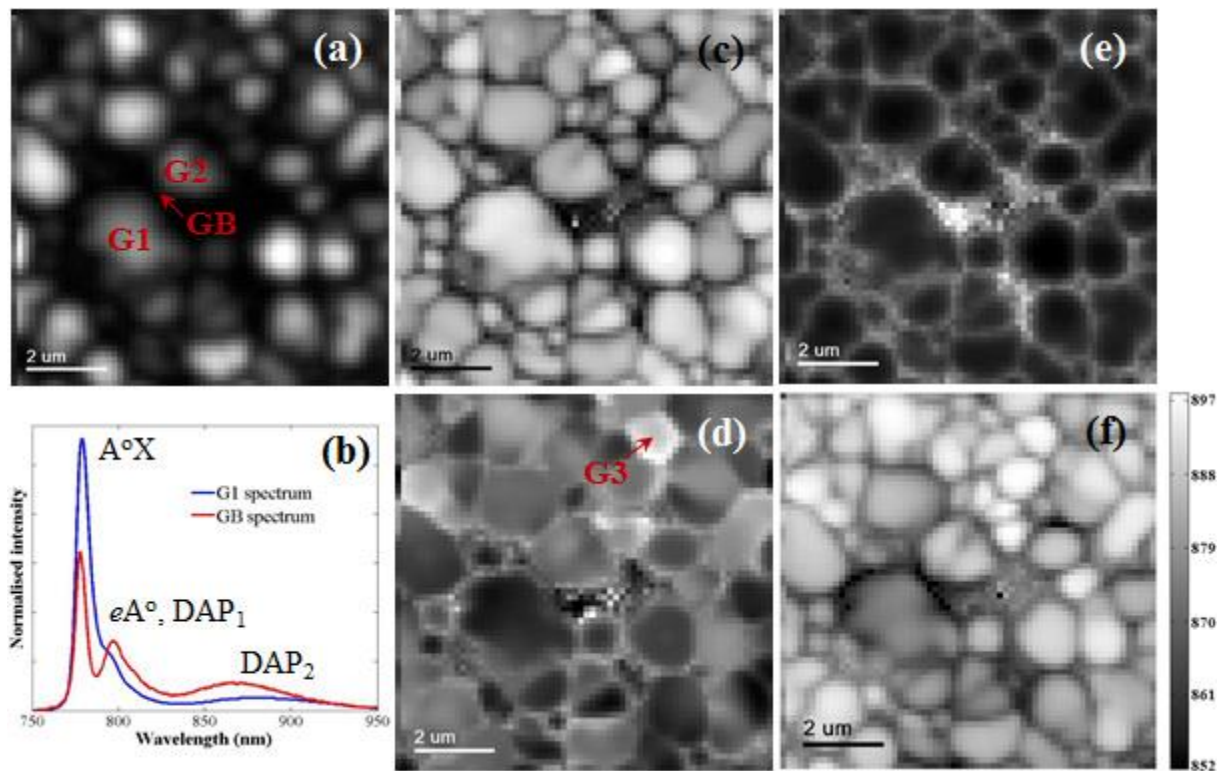


Figure 1: Continuous wave CL results from polycrystalline CdTe at 12 K. (a) is a panchromatic ‘image’ extracted from a hyperspectral map. CL spectra extracted from the grain ‘G1’ and grain boundary ‘GB’ in (a) are shown in (b); the total intensity has been normalised. Normalised intensity distributions for the $A^\circ X$, eA°/DAP_1 and DAP_2 spectral features are shown in (c), (d) and (e) respectively. The total intensity at each pixel has been normalised to remove effects of enhanced non-radiative recombination at grain boundaries. (f) shows the DAP_2 central wavelength in nanometres as a function of position. Color online.

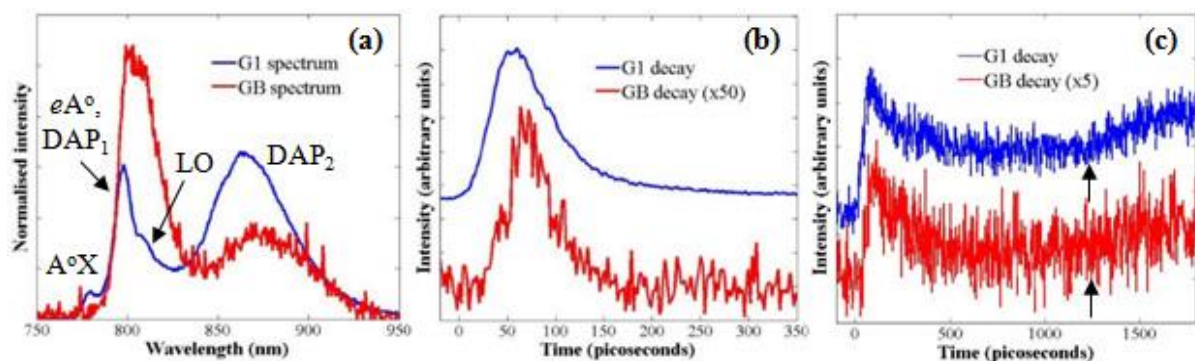


Figure 2: Pulsed CL data from polycrystalline CdTe at 12 K showing (a) time integrated spectra from G1 and GB positions in Figure 1 (total intensity has been normalised). The peak labelled ‘LO’ is the phonon replica of the eA°/DAP_1 transition. (b) and (c) show decay curves for the $A^\circ X$ and eA°/DAP_1 peaks respectively (note the difference in time scale). Color online.

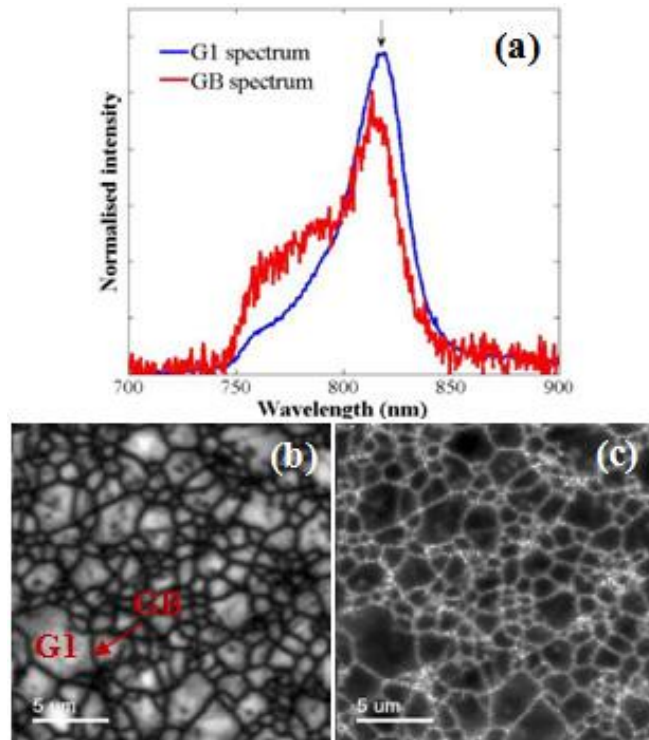


Figure 3: Room temperature, continuous wave CL from polycrystalline CdTe showing (a) spectra from a grain interior ‘G1’ and grain boundary ‘GB’; the total intensity has been normalised. (b) and (c) show the normalised (w.r.t. total signal) intensity distribution of the 818 nm (arrowed in (a)) and above band gap (i.e. 750-790 nm) emission respectively. The spatial positions ‘G1’ and ‘GB’ are indicated in (b). Color online.